Biosensors and Bioelectronics 141 (2019) 111399

Contents lists available at ScienceDirect

Biosensors and Bioelectronics

journal homepage: www.elsevier.com/locate/bios

A Portable Device for Rapid Detection of Human Serum Albumin using an immunoglobulin-coating-based Magnetoelastic Biosensor

Shengbo Sang[a], Yuchao Li[a], Xing Guo[a], Bo Zhang[a], Xianwei Xue[a], Kai Zhuo[a], Chun Zhao[b], Wendong Zhang[a], Zhongyun Yuan[a,*]

[a] MicroNano System Research Center, Key Laboratory of Advanced Transducers and Intelligent Control System of Ministry of Education and Shanxi Province, College of Information & Computer Engineering, Taiyuan University of Technology, Taiyuan, 030024, China
[b] College of Information and Communication, Sungkyunkwan University, Chunchun-Dong, Changan-Ku, 440-746, Suwon, South Korea

ARTICLE INFO

Keywords:
Portable device
Magnetoelastic (ME) biosensor
Human serum albumin (HSA)
Resonance frequency shift (RFS)
Anti-HSA immunoglobulin G (IgG)

ABSTRACT

Abnormal protein concentration levels in human body fluids, such as urine, serum etc., are considered to associate with disease states, providing essential information for the pre-clinical diagnosis. This paper presents a wireless immunoglobulin-coated magnetoelastic (ME) biosensor for fast, cost-effective detections of human serum albumin (HSA) with small sample volumes at a microliter scale. This is the first portable resonant sensor based on magnetostrictive effect that can monitor different molecular states of HSA. Anti-HSA Immunoglobulin G (IgG) was immobilized on the surface of the ME sensor to selectively capture HSA. The rapid conjugation between the antibody and antigen changed the sensor surface states and thus induced resonance frequency shifts (RFS), which were monitored in real time for the qualitative and quantitative analysis of HSA. This paper brings forward a System on Chip (SoC)-based system architecture to realize the function of RFS sampling. The performance of the portable device was validated to be comparable to that of the Vector Network Analyzer (VNA) AV3620 using different concentrations of HSA solution. The RFS were linearly proportional to the HSA concentrations in the range from 0.1 to 100 μg/mL with a linearity up to 0.998, a sensitivity of 8.70 Hz/μg.mL-1 and a detection limit of 0.039 μg/mL, indicating good feasibility of this method. Meanwhile, the response of this portable ME biosensor was quick and specific to HSA targets. This ME biosensor shows high potential to be used in diagnosing abnormal HSA.

1. Introduction

Human serum albumin (HSA) levels, which correlate with the overall HSA solution concentration, have been investigated for the early assessment of diseases (Yang et al., 2018). Many studies have confirmed that liver diseases are associated with a reduction in HSA. Rolla et al. (2000) used HSA content sensing as a core factor for liver risk diagnosis. Allarakha et al. (2016) have suggested that elevated levels of HSA antibodies were associated with diseases in diabetic subjects. An abnormal HSA content is also one of the symptoms of nephrotic syndrome and other kidney diseases (Vera Joanne and Kun-Lin, 2011). Therefore, the development of rapid and low-cost approaches for HSA measurement has attracted extensive research interest for its clinical applications (Luo et al., 2018).

The research on HSA detection in the past decades have focused on how to promote technical innovation and commercialization, such as the Bromocresol green (BCG) method (Zhou et al., 2016), the enzyme-linked immunosorbent assay (ELISA) (Rispens and Ooijevaar-de Heer, 2016), and the Bromocresol purple albumin (BCP) method (Ito, 2016). All of these approaches have typically required large sample volumes, and suffered from long measurement times, low sensitivity, high-costs, and narrow detection ranges. Normally, in the area of bio-analysis, sample volumes are available only in small quantities. Thus, there is an urgent need for HSA measurement devices that can work with a limited volume. In addition, portable and low-cost devices are highly desirable for smart applications (Guo et al., 2016).

The problems noted above have stimulated many research efforts in developing novel methods for HSA portable detection. Various micro-electro-mechanical systems (MEMS)-based biosensors have been proposed. Quartz crystal resonators (Smith et al., 2014; Yang and He, 2016; Lu and Czanderna, 2012), surface acoustic wave sensors (Nardi et al., 2012), and microcantilevers (Pietrantonio et al., 2013; Chen

* Corresponding author. MicroNano System Research Center, Key Laboratory of Advanced Transducers and Intelligent Control System of Ministry of Education and Shanxi Province, College of Information & Computer, Taiyuan University of Technology, Taiyuan 030024, China. Tel.: +86 155 3632 8195; fax: +86 351 6010029.
E-mail address: yuanzhongyun@tyut.edu.cn (Z. Yuan).

https://doi.org/10.1016/j.bios.2019.111399
Received 6 March 2019; Received in revised form 29 May 2019; Accepted 31 May 2019
Available online 01 June 2019
0956-5663/

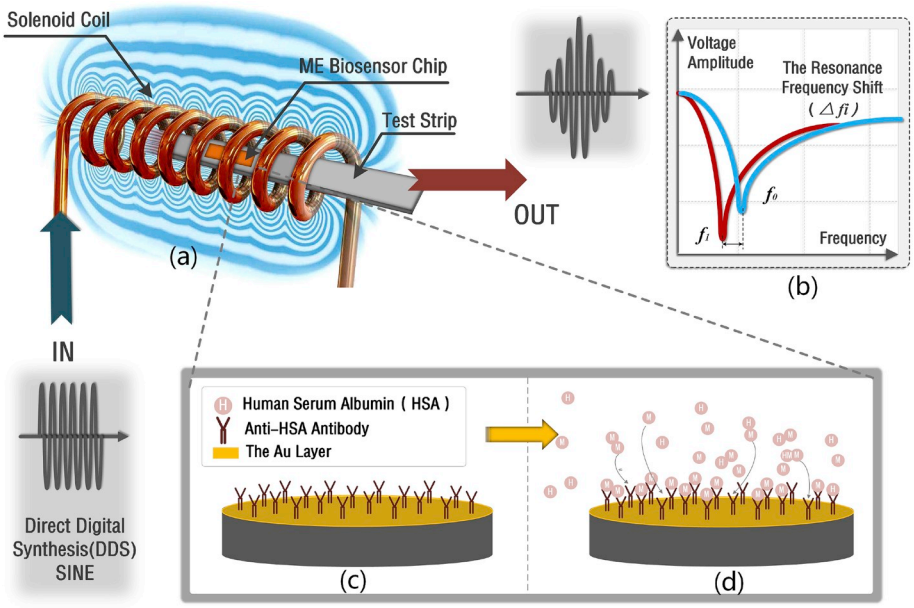

Fig. 1. Schematic diagram of the HSA measurement system and ME Biosensor Sensing mechanism. (a) The solenoid coil generates an Alternating Current (AC) magnetic field to actuate the ME biosensor chip into oscillate in the Test Strip. (b) After the combination, the RFS of ME biosensor occurs. (c) The ME sensor has a layer of the anti-HSA IgG on the surface to form ME biosensor. (d) The ME biosensor selectively adsorbs the HSA.

et al., 2016) have been developed as piezoelectric sensors. The advantages of these sensors include fast, sensitive sensing using a small volume. Among the various resonant microsensors, microcantilevers have captured a great amount of attention and have been investigated for measuring the load quality of different substances, due to their low detection limits and high sensitivity. For example, Datar R. et al. (Sohgawa et al., 2013; Datar et al., 2009; Ma et al., 2019) developed a microcantilever-based sensor for the specific detection of DNA sequences and other chemicals with in one sample. However, since they use optical equipment, the extreme complexity of the microcantilever sensor units poses a serious challenge in the manipulation of resonant parameter detection (Jie et al, 2017). Furthermore, microcantilevers have a limited degree of bending when the mass load is small, resulting in a low RFS, limiting their usage due to low load quality.

As a new category of resonating sensors, ME biosensors detect HSA based on the magnetostrictive effect, which produces a reliable detection of the internal resonance on the sensing chip (Chen et al., 2017; Li et al., 2012). The process takes advantage of simple instrumentation and is highly efficient. In addition, ME biosensors can be easily miniaturized. The ME biosensor chip consists of a micro-sized chip of amorphous ferromagnetic alloy (RAFA) that oscillates along its length direction (Nowicki, 2018). Depending on vibration in the longitudinal mode (Zhang et al, 2014), ME biosensors have on high operational sensitivity, making it suitable in the detection of a wide range of solution concentrations. Furthermore, Sokolov et al. showed that the fabrication cost of a single ME sensor was less than 1/100,000 of one US Dollar (USD), making the sensors disposable economically (Sokolov et al., 2009).

Various instruments have been introduced that can be relayed on the ME biosensor model. Holmes et al. (2012) were among the early researchers that produced on applicability study of ME sensors based on the simple ME structure. Hiremath et al. (2015) tested the quality of bacteria using a multiple immunoglobulin coating on an ME biosensor. The ME biosensor has been employed to detect heavy metal ions for monitoring human health and to prevent cancer, neurodegenerative diseases, cardiovascular disease and nervous system failure (Guo et al., 2018; Ma et al., 2015; Verma and Gupta., 2015). In the various ME biosensor studies mentioned, the ME biosensors were biologically molecule-functionalized with antigen-antibody complexes to qualitatively assess the level of bacteria, viruses, decomposed organics (Maria Encina AulloMaestro et al., 2017), and other parameters (Nguyen et al., 2019). Furthermore, an ME sensor can determine the mass of a substance based on the RFS.

In this study, an immunoglobulin-based ME biosensor has been demonstrated to successfully measure HSA in the light of a quantitative assay, thereby providing early warnings for potential patients that may prevent the occurrence of certain diseases. In addition, the proposed biosensor has a system architecture based on the SoC processor (ARM Cortex M-3 core) as the primary controller. This biosensor features simple hardware, low-power consumption, good real-time detection, low detection limits, and a compact system construction that makes it suitable for rapid medical diagnosis. In this study, the performance of the detection system was characterized using sample solutions with various ratios. The resonant frequency of the ME modified biosensor against the HSA concentration was systematically measured. Finally, the capability of measuring the HSA concentration using the portable ME biosensor system has been confirmed.

2. Theory and related work

The ME biosensor is a freestanding micro-rectangular chip fabricated from a high-strength ME superalloy. Under the function of an alternating magnetic field, the ME biosensor oscillates along its length. When the ME biosensor vibrates at a characteristic resonance frequency, the mechanical vibration reaches its maximum. Correspondingly, the mechanical vibration of the ME biosensor induces a change in the magnetic flux, that is sensed by a pick-up coil (Laistler and Moser, 2018).

Fig. 1, shows a schematic diagram of the developed HSA detection system based on an ME biosensor and a solenoid coil. To measure the RFS of the ME biosensor, the chip is placed in a test slot and inserted into the solenoid coil. The length direction of the solenoid coil is perpendicular to the coil turns, as shown in Fig. 1a. The direct digital synthesis (DDS) generates a sweep signal that acts on the solenoid coil. When the ME biosensor vibrates at a characteristic resonance frequency, the induction voltage of the solenoid coil is at its minimum, which can be sensed by a pick-up coil. The anti-HSA IgG is immobilized on the surface of the ME sensor to form the ME biosensor. The ME biosensor is used to selectively adsorb the HSA at 37 °C. Due to the combination of the anti-HSA IgG and HSA antigen, the extra load mass on the ME biosensor increases, which in turn causes the resonance frequency to decrease (Kubo et al., 2015).

The magnetic energy converts into elastic energy, depending on the strength of ME biosensor vibrates. In this case, vibration is at the

resonance frequency, which results in maximum string vibration. Meanwhile, the output voltage on pick-up coil achieves its minimum (Xu and Zhao, 2017). Therefore, the pick-up coil continues sampling until it is under the frequency of resonance. We can detect different amplitudes of voltage by an oscilloscope. Based on the ME biosensor with a length of L, width of W and height of H, the resonant frequency (f_0) of longitudinal vibration in slot is expressed as (Sang et al., 2016):

$$f_0 = \frac{1}{2L}\sqrt{\frac{E}{\rho(1-\sigma^2)}} \tag{2.1}$$

where E, σ and ρ are the Young's modulus, Poisson's ratio and density, respectively. Due to the Antigen-antibody complexes, the extra load mass on the ME biosensor increases, which in turn causes the resonance frequency decrease, as shown in Fig. 1b. By correlating the RFS to the concentration of the determinant, the mechanism of ME biosensors can be established When the test temperature is constant, the resonance frequency of the ME sensor is sensitive to the mass change on its surface. For an extra load mass of Δm on the ME biosensor with a mass M, the RFS (Δf_i) is expressed as (Hiremath et al., 2015; Schmidt and Grimes, 2001):

$$\Delta f_i = -\frac{f_0}{2M}\Delta m \tag{2.2}$$

Form Eq. (2.2), the RFS (Δf_i) is proportional to the load mass of HSA. As shown in Fig. 1d, the anti-HSA IgG is immobilized on the surface of the ME biosensor to selectively adsorb the HSA. Since the Antigen-antibody complexes, the extra load mass on the ME biosensor increases, which in turn causes the resonance frequency decrease. Finally, the HSA can be detected by monitoring the resonance frequency of the ME biosensor.

3. Implementation and measurement

3.1. Preparation of the ME biosensor

The ME biosensor chip is composed of a Metglas alloy 2826 MB ($Fe_{40}Ni_{40}P_{14}B_6$), which is in a strip-shaped form with a thickness of 28 μm. In this study, the ribbon was diced into rectangular strips for use as freestanding ME biosensors chips with the geometrical parameters of 1 mm × 5 mm × 28 μm, as shown in Fig. 2c. The gold-coated sensor was cleaned using an ultrasonic cleaning device in an acetone solution for 10 min, followed by ultrasonic cleaning using isopropanol, anhydrous ethanol, and deionized water for 10 min each. The sensor was immersed in a 40 mmol/L cysteamine (CYS) solution for 12 h at room temperature to form a self-assembled monolayer. The unbonded thiols were then removed from the modified sensor by rinsing several times in ethanol. An antibody solution of 200 μg/mL was diluted to 25 μg/mL using a phosphate buffered saline (PBS) solution of 140 μL. Then, it was dipped into a solution that contained 1-ethyl-3-(3-dimethylaminopropyl) carbodiimide (EDC) and N-hydroxysulfosuccinimide (NHS) for 30 min to convert the active carboxylic terminal groups to an NHS-ester. Then, the modified sensor was immersed in an anti-HSA IgG solution at 37 °C for 1 h. Finally, the ME biosensor was formed, as shown in Fig. 2c. The CYS, PBS, EDC, and NHS were purchased from Sigma Aldrich (USA). Anti-HSA IgG was purchased from the Shanghai Yugong Biotechnology Co., Ltd.

Two test slots exist on the test strip of the ME biosensor for a reference chip and a sensing chip. The slots are slightly larger than the ME biosensor due to the 3D printing process, as shown in Fig. 2a. During the concentration measurement, ME biosensors were placed in this slot, which positions the sensor chip and prevents the chip moving in the coil. After that, the test strip was inserted into the middle of the solenoid coils. A numerical simulation and the experimental validation were used to study this relationship. The simulation results showed that along the central axis of the coil, the magnetic induction in the middle was much larger than in the two ends, regardless of the position of the excitation section. Hence, the middle of the coil was the best detection position for the ME biosensor (Sang et al., 2015; Wei et al., 2013; Wei, 2013). In the solenoid coils, the copper wire is adjacent to a glass tube of 3 mm in diameter. The apparent peak in the resonance appeared by choosing the rational parameters of the coil. In this design, the number of coil turns was 200, and the length of coil line was 20 mm, as shown in Fig. 2b.

AFM scans (typically 1 μm × 1 μm) were carried out on several surface positions to check the surface uniformity. Fig. 2d shows the scans result on the sample that immobilized anti-HSA IgG (labeled as antibody). The average peak to valley height was 40.0 nm. After the anti-HSA IgG is immobilized on the surface of the ME sensor, the ME biosensor selectively adsorbs the HSA. Fig. 2e shows that the appearance of peaks has a uniform and homogenous distribution on the

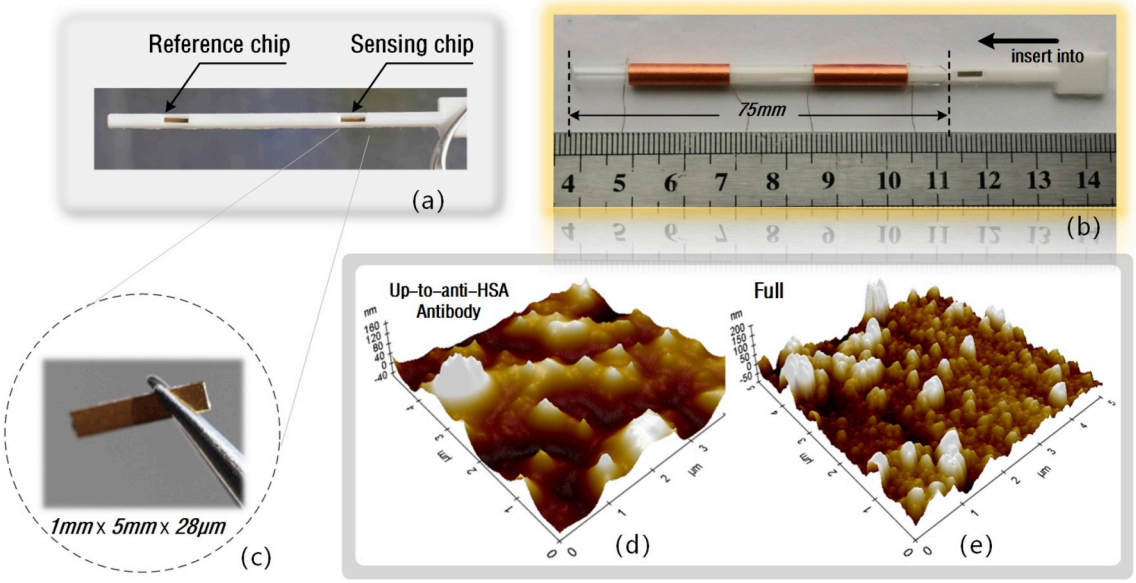

Fig. 2. (a) Two test slots for ME biosensors chips including reference chip and sensing chip. (b) The components and the assembly process of the ME biosensor. (c) The photograph of sensing chip and parameters 1 mm × 5 mm × 28 μm; The AFM image of the surface of the ME biosensor (d) before the combination of the anti-HSA IgG and HSA antigen and (e) after the combination.

surface (labeled as Full). Due to the combination of the anti-HSA IgG and HSA antigen, the average peak to valley height was about 100.0 nm. The experimentally confirm that the average peak to valley height has obviously change modifications of the surface morphology occurred.

3.2. Sensing mechanism

The ME biosensor is inserted into an air-cored solenoid coil, and an AC excitation signal acts on the coil. Due to the AC magnetic field, the coil drives the ME biosensor to oscillate, and the higher the AC current, the stronger the vibration. This causes a maximum in the mechanical energy at the resonance frequency. In contrast, the direction of the bias magnetic field is perpendicular to the pick-up coil, which eliminates the effect of frequency doubling. Based on the impedance detuning technique (Zhao et al., 2012; Grimes et al., 2011), the vibration amplitude and phase are measured as a function of frequency, and the impedance is measured by the pick-up solenoid. Along with magnetic-flux increases, the ME biosensor achieves a condition of resonance, while a significant sharp peak occurs in the solenoid impedance spectrum. Hence, in terms of this sharp peak, the resonance frequency of the ME biosensor can be measured, and our sampling strategy as shown in Fig. 3.

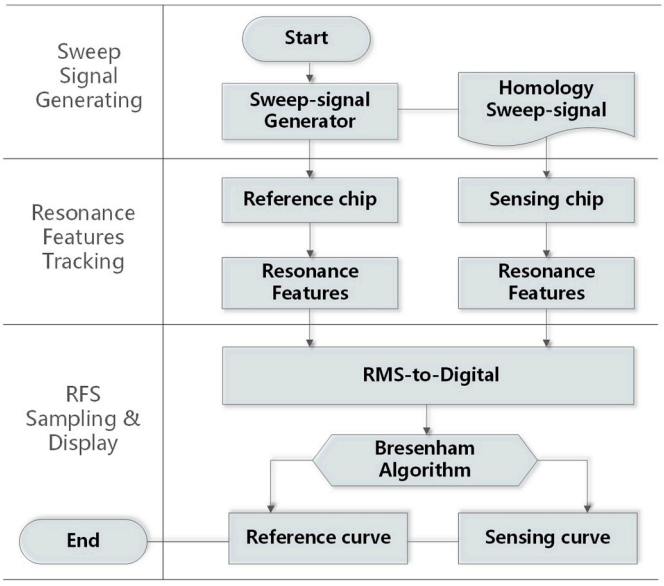

Fig. 3. Flow chart of the induced system detection strategy.

STEP1. Sweeping Signals. After the initialization, sweeping signals are implemented using a software-defined radio (SDR). By programming a microprogrammed control unit (MCU), virtual ME resonance modules were built using two discrete components. By the use of sweeping signal switching, the MCU redistributes these sine pulses to each probe (driver coil) and establishes an excitation sequence for parallel measurements.

STEP2. Resonance Feature Tracking. The MCU also includes sampling functional blocks, such as a microcontroller with ME resonance (MR) modules, internal data storage, and other functional blocks. After each sine pulse, the resulting MR signal is recorded, and two signals (on a reference chip and a sensing chip) are digitally converted into the MCU.

STEP3. Results Exhibition. The MCU processes the acquisition data, to provide information in the external FLASH. Using Bresenham algorithm optimization, the acquisition data can be displayed on a screen. Using two display channels, users can compare the two analysis results obtained from the reference and sensing chips, and confirm the HSA detection.

3.3. Hardware implementation

In this study, a portable HSA detection system was implemented using an ARM-based SoC component. The DDS generated the sweep signal that acted on the solenoid coil. Improvements were made to certain elements of this circuit, such as a new microcontroller that had a 12-bit multi-channel analog to digital converter on the chip, and a display. A diagram of the circuit design is shown in Fig. 4. The key components and processes of the device are the following:

MCU module: The STM32F103RCT6 chip has been adopted as the main control chip in this system. As a production of 32-bit processor, STM32F103RCT6 (Basic-Frequency: 72 MHz) is based on ARM Cortex-M3 architecture. It supports single-cycle DSP instructions and floating-point calculation, on-chip integrating 12-bit successive approximation analog-to-digital converters (ADC), SRAM (48 KB) and FLASH (256 KB). There are several features including low-power consumption (1.9 μA/MHz), Mini-size, low-cost, high reliability and compatibility. According to Nyquist sampling theorem $f_s \geq 2f_{i\max}$, where f_s and $f_{i\max}$ are the sampling frequency and the frequency of the highest frequency component of the input signal. In this design, due to $f_{i\max} = 450$ KHz, the single sampling rate is set $f_s = 2.4$ MHz.

DDS: The AD9850 generates a frequency/phase-agile sine wave using DDS technology, in the form of a numerically controlled oscillator. DDS is in the form of a numerically controlled oscillator that allows fast and precise manipulation of its output frequency under full digital control. In our case, the AD9850 employed a serial load mode that simulates a sine wave range from 444.000 kHz to 464.480 kHz, and a synthesized wave with a frequency resolution of 0.0291 Hz.

RMS-to-DC converter: A root-mean-square to direct current (RMS-to-DC) converter is used to enable the internal analog-to-digital (AD) converter of the MCU sample analysis. An RMS-to-DC converter, AD536A, is used to compute the true root-mean-square (RMS) value of the AC signal. It is a complete monolithic integrated circuit that performs a true RMS-to-DC conversion. The AD536A has a 450 kHz bandwidth and performs the RMS-to-DC conversion with the aid of an external capacitor.

Others: A Direct Current (DC) biasing magnetic field can be provided by the magnet that makes the sensor from an optimal operational point of view, to facilitate sensor excitation. The Serial Flash memory (W25Q128BV 16 MB) provides an extended storage solution for systems. The power system support 3.3v and 5V by lithium batteries. A display (solution 350 pixel*240 pixel) is selected to display the independence spectrum curve, resonance frequency and other parameters.

4. Results and discussion

In a healthy individual, the levels of kidney HSA is less than 30 μg/mL in urine albumin. In a clinical diagnosis, it ranges from 30 to 100 μg/mL of urine albumin in a state of kidney injury (Alino et al., 2011). The real-time responses of the immune reaction on the ME biosensor surface (as a response function of the immersion time) based on HSA (purchased from Shanghai Yugong Biotechnology Co., Ltd.) concentrations varying from 0.1 to 100 μg/mL is tested. After the ME biosensor was immersed in the HSA suspension at 37 °C, an immune reaction was activated between the immobilized antibody and the HSA antigen. This type of situation resulted in the HSA molecule binding on the biosensor surface, and the anti-HSA IgG proportionately combined with the HSA antigen. In addition, a considerable increase in the mass on the surface caused a decrease in the resonance frequency of the ME biosensor after an initial period of induction. Normally, this experiment would require an induction time. The RFS of the ME biosensor at different HSA concentrations were calculated as the frequency difference between the varied concentrations and 0 μg/mL of HSA. At each concentration, the RFS of the ME biosensor was monitored and recorded for 40 min at intervals of 5 min. The steady-state response can was

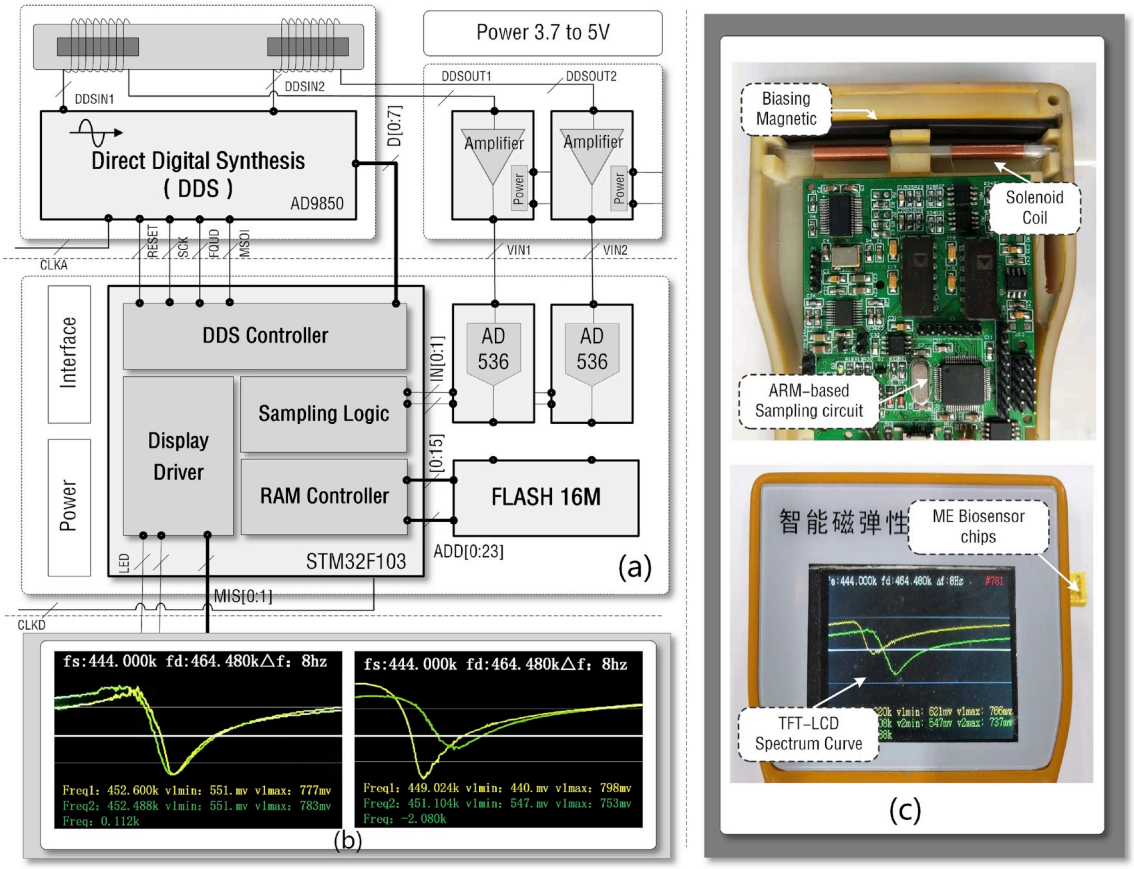

Fig. 4. (a) A portable system structure of our rapid HSA detection. (b) The RFS change of ME biosensor before and after the combination of the anti-HSA IgG and HSA antigen. (c) The components of the sensing system including Biasing Magnetic, Solenoid coil, ARM-based Sampling circuit, ME Biosensors strip and Display.

achieved in 40 min (see Fig. S1a in Supplemental Information).

The performance of the ME biosensor-based mass-sensing chip for HSA detecting was characterized. By adjusting the concentration of the HSA, the test solutions had a wide concentration range. Fig. 5a shows the resonance spectra of the ME biosensor combination of the anti-HSA IgG and HSA antigen. In addition, the resonant frequency of the ME biosensor and the resonant amplitude decreased, due to an increase in the HSA concentration from 0.1 to 100 μg/mL. To determine the resonance parameters, the measured voltage spectrum was fitted using the Lorentz function. According to the fitting results in Fig. 5a, the resonance frequency parameter of the ME biosensor was calibrated to the HSA concentration. In this experiment, the chip with an HSA concentration of 0 μg/mL was used as the reference. To demonstrate that the response of the ME biosensor was only because of the specific binding to HSA, a contrast experiment was conducted without HSA (PBS curve) which exhibited a noise level of ~70 Hz due to nonspecific binding. Nevertheless, the RFS of the ME biosensor was 300-Hz at the 0.1 μg/mL HSA concentration. Hence, an indistinctive RFS occurred without specific binding between the anti-HSA antigen and HSA.

To investigate the specificity of the ME biosensor towards different proteins, the specificity was tested by determining the ME biosensor responses to immunoglobulins light chain (IGL), human β2-micro globulin (β2-MG), albumin from bovine serum (BSA), hemoglobin (HGB), and lysozyme (LZM), each at concentrations of 10 μg/mL. The IGL, β2-MG, HGB and LZM were purchased from the Shanghai Fanke Biological Technology Co., Ltd. The BSA was purchased from Sigma Aldrich (USA). The ME biosensor exhibited an insignificant response to these selected interferences because of non-specific absorption, with response levels familiar to the blank sample PBS. The results confirmed that the RFS was due to the specific binding of the HSA and anti-HSA IgG modified on the biosensor surface (see Fig. S2 in Supplemental Information). Furthermore, the ME biosensor exhibited strong specific binding to HSA antigen, illustrating the potential feasibility for actual HSA detection. Matrix effect was evaluated according to the following equation (D. Moreno-Gonzalez et al., 2017; Jia et al., 2016):

$$\text{Matrix effect} = \left(\frac{A}{B} - 1\right) \times 100\% \tag{4.1}$$

where A is the calibration curve slope in matrix and B is the calibration curve slope in solvent.

In this study, matrix effect was estimated for each concentration of 10 μg/mL and 100 μg/mL in the mixture sample and pure sample. To evaluate the matrix effect in the proposed method, the calibration curves in standard solution (pure sample) and in sample matrix (mixture) obtained from the linear analysis were compared. The matrix effect of the portable device were −1.65% and −9.76% (see Table S2 in Supplemental Information). Matrix effect was lower than |15|% which involves that the proposed sample treatment is enabled to remove co-interferences in studied cases which indicated no significant matrix effects (Wan et al., 2018). Therefore, matrix effects were negligible in studied cases, so that the use of matrix-matched calibration would not be mandatory when the portable device was used to analyze HSA in complex biological samples accurately. In tiny detecting chamber, with the increasing concentration, the viscosity of the mixture becomes higher, which has been reported in our previous work (Sang et al., 2016; Peng et al., 2015). There is a negligible difference in viscosity between the mixture and the single HSA at a concentration of 10 μg/mL. Therefore, the frequency responses are almost the same. However, because of biological macromolecules (IGL, β2-MG, HGB, LZM, HSA), there is a little difference in viscosity between the mixture and the single HSA at a concentration of 100 μg/mL system, resulting in a

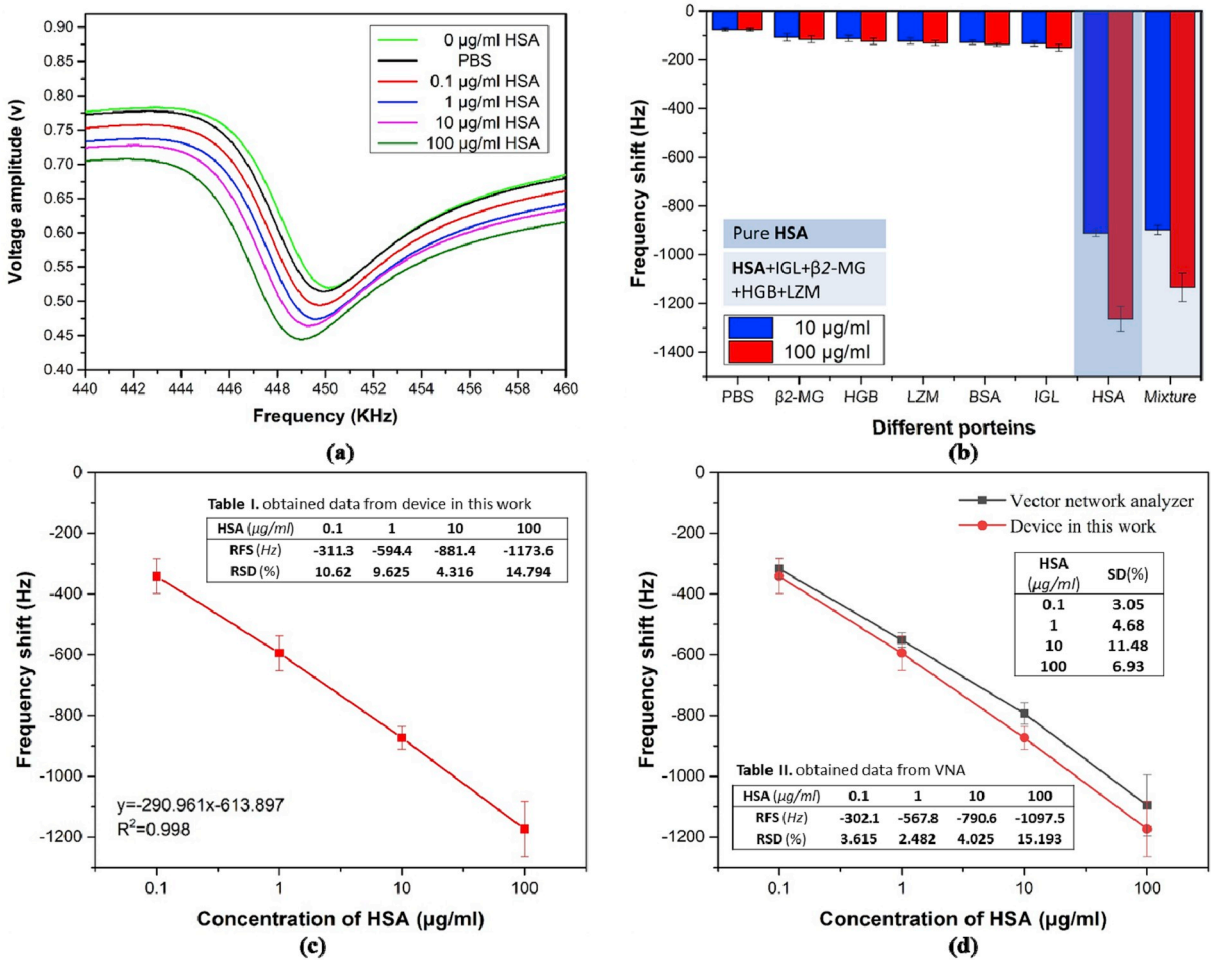

Fig. 5. (a) The resonance spectra of the ME sensor combination of the anti-HSA IgG and different HSA antigen concentrations. (b) Response of the ME biosensor to other interferences with the concentration of 10 μg/mL and 100 μg/mL, respectively. (c) A function of concentration of HSA and frequency shift, and the Goodness of Fit is equal to 0.998. (d) Compared with the results of the VNA AV3620 with the same chip.

Table 1
Performance of this method compared to other HSA biosensors.

HSA biosensors	LOD(μg/mL)	Linear range(μg/mL)	References
Fluorescent HSA sensor	1.23	0–100	Da-Jun et al. (2018)
High-selective HSA sensor	0.30	0–500	Xu et al. (2018)
Near-infrared fluorescent sensor	8.4	0–1000	Fan et al. (2016)
Rapid-response fluorescent sensor	1.91	0–100	Li et al. (2018)
Our biosensor	0.039	0–100	This work

significant difference of frequency responses, as shown in Fig. 5b. The resonant frequency amplitude decreases, while the RFS increases with an increase of the HSA concentration. The analyzed data were obtained by averaging the results of experiments. Compared with the results of the VNA AV3620, the precision of this device is close to that of a standard device, but the overall dimension is approximately 1/40 the size of the AV3620. The concentration variation of the HSA antigen solutions varied from 0.1 μg/mL to 100 μg/mL. Fig. 5d shows a comparison of the RFS between the VNA and the device in the work. Fig. 5c shows that the RFS follows a linear relationship with the HSA solution concentration. The results in Fig. 5c indicate that the RFS of the ME biosensor depends on the concentration of HSA antigen solutions. In the linear region, the sensing sensitivity determined using the RFS is approximately 8.70 Hz/μg.mL-1. Due to the high sensitivity, this method is appropriate for HSA detection. The concentration of HSA was obtained using the calibrated function: $X = (Y+613.897)/(-290.961)$, where X and Y are the HSA concentration and RFS, respectively. By comparing the goodness of fit of the two linear $R^2 = 0.998$, the principle of the method was proven. The stability of the ME biosensor was investigated by determining the RFS, which was stored in a refrigerator at 4 °C. Similarly, the stability of the ME biosensor was tested over the course of seven days using seven ME biosensors independently, each at a concentration of 10 μg/mL and 100 μg/mL. The obtained values exhibited no distinct changes, and the developed ME biosensor had an acceptable relative standard deviation (RSD) = 0.57% and RSD = 0.46% (see Fig. S1b in Supplemental Information), for each concentration. The stability was attributed to the fact that the HSA was firmly attached on the surface of the ME biosensor. Compared with other biosensors (Da-Jun et al., 2018; Xu et al., 2018; Fan et al., 2016; Li et al., 2018) for HSA detection presented in Table 1, the proposed ME biosensor showed an equal or better performance. The limit of detections (LODs) of HSA were nearly entirely in the range of microgram per

milliliter units. Under the premise that the linear range is nearly the same, the ME biosensor in this work showed a better detection limit. Additionally, the proposed method in this work has a greater potential for miniaturization and creation of biosensors for individual use because it does not require complex and expensive devices (such as a VNA).

Therefore, according to the RFS, the ME biosensor can distinguish varying concentrations of HSA. The results demonstrated that the detection device based on ME biosensing is suitable for rapid screening of patients with abnormal concentrations of HSA solution.

5. Conclusion

In conclusion, a novel portable ME biosensor device was designed and fabricated based on SoC processor. This sensing device is small, cost-effective, stable, and able to detect HSA rapidly and specifically, with a detection limit as low as 0.039 μg/mL. The superior performance relied on magnetostrictive effect in the RFS of the ME biosensor, of which the chamber was modified with anti-HSA IgG. The selective conjugation of HSA led to the load mass increase, which in turn caused the resonance frequency decrease. The results verified that this ME biosensor can accurately determine the concentrations of HSA in the linear range of 0.1–100 μg/mL. Our ongoing work is to integrate the current device with sampling units to purify the clinical samples. This novel portable device has high potential for pre-clinical diagnosis of HSA. With the same strategy, it can detect other proteins by using specific antibodies for the analysis of biomedical information.

Declaration of interest statement

We declare that we have no financial and personal relationships with other people or organizations that can inappropriately influence our work, there is no professional or other personal interest of any nature or kind in any product, service and/or company that could be construed as influencing the position presented in, or the review of, the manuscript entitled, “A Portable Device for Rapid Detection of Human Serum Albumin using an Immunoglobulin-coating-based Magnetoelastic Biosensor”.

CRediT authorship contribution statement

Shengbo Sang: Writing - original draft, Formal analysis. **Yuchao Li:** Writing - original draft, Formal analysis. **Xing Guo:** Formal analysis. **Bo Zhang:** Formal analysis. **Xianwei Xue:** Data curation. **Kai Zhuo:** Investigation. **Chun Zhao:** Resources. **Wendong Zhang:** Funding acquisition. **Zhongyun Yuan:** Writing - original draft, Formal analysis.

Acknowledgements

The research was partially supported by the National Natural Science Foundation of China (No. 51622507, 61471255, 61474079, 61501316, 51505324), Excellent Talents Technology Innovation Program of Shanxi Province of China (201605D211023,201805D211020).

Appendix A. Supplementary data

Supplementary data to this article can be found online at https://doi.org/10.1016/j.bios.2019.111399.

References

Aliño, V.J., Yang, K.-L., 2011. Analyst 136 (16), 3307–3313.
Allarakha, S., Dixit, K., Zaheer, M.S., Siddiqi, S.S., Moinuddin, Ali A., 2016. Int. J. Biol. Macromol. 88, 93–101.
Chen, X., Pan, Y., Liu, H., Bai, X., Wang, N., Zhang, B., 2016. Biosens. Bioelectron. 79, 353–358.
Chen, P., Jiang, Q., Horikawa, S., Li, S., 2017. J. Electrochem. Soc. 164 (6), B247–B252.
Da-Jun, Z., Jing, X., Mi-Mi, S., Zhi-Gang, S., Qing-Cai, J., Yu-Shun, Y., Hai-Liang, Z., 2018. Sensor. Actuator. B Chem. 271, 82–89.
Datar, R., Kim, S., Jeon, S., Hesketh, P., Manalis, S., Boisen, A., Thundat, T., 2009. MRS Bull. 34 (6), 449–454.
Fan, X., He, Q., Sun, S., Li, H., Pei, Y., Xu, Y., 2016. Chem. Commun. 52 (6), 1178–1181.
Grimes, C.A., Roy, S.C., Rani, S., Cai, Q., 2011. T Sensors 11 (12), 2809–2844.
Guo, X., Gao, S., Sang, S., Jian, A., Duan, Q., Ji, J., Zhang, W., 2016. Biosens. Bioelectron. 82, 127–131.
Guo, X., Sang, S., Jian, A., Gao, S., Duan, Q., Ji, J., Zhang, Q., Zhang, W., 2018. Sensor. Actuator. B Chem. 256, 318–324.
Hiremath, N., Guntupalli, R., Vodyanoy, V., Chin, B.A., Park, M.K., 2015. Sensor. Actuator. B Chem. 210, 129–136.
Holmes, H.R., Tan, E.L., Ong, K.G., Rajachar, R.M., 2012. Biosensors 2 (1), 57–69.
Ito, S., 2016. Curr. Pharm. Anal. 12 (1), 25–29.
Jia, X., Zhao, P., Ye, X., Zhang, L., Wang, T., Chen, Q., Hou, X., 2016. Talanta 169, 227–238.
Jie, W., Zhang, H., Xie, Y., Yan, Z., Ying, Y., Long, H., Cui, X., Min, G., Su, Y., Yang, W., 2017. Nano Energy 33 (Complete), 418–426.
Kubo, T., Arimura, S., Tominaga, Y., Naito, T., Hosoya, K., Otsuka, K., 2015. Macromolecules 48 (12) 150601143133004.
Laistler, E., Moser, E., 2018. Nat. Biomed. Eng. 2 (8), 557–558.
Li, S., Horikawa, S., Park, M.K., Chai, Y., Vodyanoy, V.J., Chin, B.A., 2012. Intermetallics 30(none). 0-0.
Li, P., Wang, Y., Zhang, S., Liang, X., Wang, G., Cui, J., 2018. Tetrahedron Lett. 59 (14) S0040403918302600.
Lu, C., Czanderna, A.W., 2012. Elsevier 7.
Luo, Z., Liu, B., Zhu, K., Huang, Y., Pan, C., Wang, B., Wang, L., 2018. Dyes Pigments 152, 60–66.
Ma, X., Truong, P.L., Anh, N.H., Sim, S.J., 2015. Biosens. Bioelectron. 67, 59–65.
Ma, X., Song, S., Kim, S., Kwon, M.-s., Lee, H., Park, W., Sim, S.J., 2019. Nat. Commun. 10 (1), 836.
Maria Encina AulloMaestro, Hunter, P., Spyrakos, E., Mercatoris, P., Kovács, Attila, Horváth, Hajnalka, Tom, Preston, Matyas, Presing, Palenzuela, Jesus Torres, Tyler, Andrew, 2017. Biogeosciences 14 (5), 1–41.
Moreno-Gonzalez, D., Hamed, A.M., Garcia-Campana, A.M., Gamiz-Gracia, L., 2017. Talanta 171, 74–80.
Nardi, D., Zagato, E., Ferrini, G., Giannetti, C., Banfi, F., 2012. Appl. Phys. Lett. 100 (25), 119.
Nguyen, A.H., Ma, X., Park, H.G., Sim, S.J., 2019. Sensor. Actuator. B Chem. 282, 765–773.
Nowicki, M., 2018. Sensors 18 (12), 4420.
Peng, C., Shuang, G., Zhang, W., Tao, W., Jian, A., Sang, S., 2015. Smart Mater. Struct. 24 (4) 045029.
Pietrantonio, F.D., Cannatà, D., Benetti, M., Verona, E., Varriale, A., Staiano, M., D'Auria, S., 2013. Biosens. Bioelectron. 41 (1), 328–334.
Rispens, T., Ooijevaar-de Heer, P., 2016. J. Immunol. Methods 430, 61–63.
Rolla, R., Vay, D., Mottaran, E., Parodi, M., Traverso, N., Aricó, S., Sartori, M., Bellomo, G., Klassen, L.W., Thiele, G.M., 2000. Hepatology 31 (4), 878–884.
Sang, S., Cheng, P., Zhang, W., Li, P., Hu, J., Li, G., et al., 2015. J. Intell. Mat Syst. Strat. 26 (8), 980–987.
Sang, S., Gao, S., Guo, X., Cheng, P., Zhang, W., 2016. Appl. Phys. Lett. 108 (5) 054102.
Schmidt, S., Grimes, C.A., 2001. Sens. Actuators, A 94 (3), 189–196.
Smith, S.E., Williams, J.M., Ando, S., Koide, K., 2014. Anal. Chem. 86 (5), 2332–2336.
Sohgawa, M., Fujimoto, T., Takada, K., Yamashita, K., Noda, M., 2013. Sensors 1–14.
Sokolov, A.N., Roberts, M.E., Bao, Z., 2009. Mater. Today 12 (9), 12–20.
Vera Joanne, A.O., Kun-Lin, Y., 2011. Analyst 136 (16), 3307–3313.
Verma, Roli, Gupta, B.D., 2015. Food Chem. 166, 568–575.
Wan, Y.C., Liu, Y.J., Liu, C., Ma, H.T., Yu, H.F., Kang, J.W., Gao, C.L., Wu, Z.Q., Zheng, D., Lu, B., 2018. J. Pharm. Biomed. 154 S0731708517328959.
Wei, X.J., 2013. Tai Yuan University of Technology Master's Thesis.
Wei, X.J., Sang, S.B., Zhang, W.D., Cheng, P., Cheng, C.Q., Li, P.W., Hu, J., Li, G., 2013. Key Eng. Mater. 339–343.
Xu, H., Zhao, Y., 2017. 2017 IEEE 2nd IAEAC. pp. 783–787.
Xu, Y.-J., Su, M.-M., Li, H.-L., Liu, Q.-X., Xu, C., Yang, Y.-S., Zhu, H.-L., 2018. Anal. Chim. Acta 1043, 123–131.
Yang, M., He, J., 2016. Sensor. Actuator. B Chem. 228, 486–490.
Yang, R.-J., Tseng, C.-C., Ju, W.-J., Wang, H.-L., Fu, L.-M., 2018. Chem. Eng. J. 352, 241–246.
Zhang, H., Yang, Y., Su, Y., Chen, J., Zhong, L.W., 2014. Adv. Funct. Mater. 24 (10), 1401–1407.
Zhao, T., Minerbo, G., Hunka, J., Goswami, J.C., 2012. Antennas & Propagation Society International Symposium.
Zhou, L., Lv, Z., Jing, S., Ying, X., Luo, X., Zhang, Y., Yang, H., Zhang, W., Luo, S., Fang, J., 2016. J. Clin. Lab. Anal. 30 (5), 581–589.